pH-Controlled Gliding Motions in Pillar[5]arene-Containing Molecular Shuttles

Nihed Becharguia, Iwona Nierengarten, Alix Sournia-saquet, Emeric Wasielewski, Rym Abidi, Béatrice Delavaux-nicot, Jean-françois Nierengarten

ChemistryEurope
Excellence in Chemistry Research Worldwide

Research Article
doi.org/10.1002/ceur.202400115

www.journal.chemistry-europe.org

pH-Controlled Gliding Motions in Pillar[5]arene-Containing Molecular Shuttles

Nihed Becharguia, Iwona Nierengarten,* Alix Sournia-Saquet, Emeric Wasielewski, Rym Abidi, Béatrice Delavaux-Nicot,* and Jean-François Nierengarten*

Dedicated to the memory of Dr. Claude Sirlin

New pillar[5]arene-based molecular shuttles incorporating an axle component with two stations, namely a $-(CH_2)_{10}-$ chain and a protonable triazole subunit, have been prepared. Detailed spectroscopic investigations supported by density functional theory calculations revealed that gliding motions of the pillar[5]arene occur over the full length of the molecular axle in the protonated state, while such molecular motions are limited over the decyl station in the neutral state. Finally, electrochemical investigations further revealed that the oxidation of the pillar[5]arene moiety of the protonated rotaxane also triggers conformational changes and the oxidized macrocycle is only located over the decyl station.

1. Introduction

Owing to large amplitude molecular motions observed in rotaxanes, this class of compounds has attracted particular attention for the construction of molecular machines.[1–3] Typically, the axle moiety of the rotaxane contains two or more distinct binding sites or stations for its macrocyclic component.[3] The relative affinity for the different stations can be modulated and the Maxwell–Boltzmann distribution of co-conformers differing by the position of the macrocycle on its axle can be inverted by using an appropriate chemical, electrochemical, or optical stimulus.[3] As part of our research program on pillar[5]arene-containing rotaxanes, uncontrolled dynamic gliding motions of the macrocyclic subunit along its axle unit have been investigated in details.[4,5] Based on all the knowledge acquired from our previous systems, we now propose to use our building blocks for the preparation of [2]rotaxanes in which the position of the macrocycle can be controlled by an external stimulus. So far, only a few examples of pillar[5]arene-based molecular shuttles have been reported.[6,7] Actually, when compared to related systems prepared with other macrocycles,[3] a perfect conformational control is by far more difficult to achieve owing to the low interaction energies between the different stations of the axle and the pillar[5]arene subunit.[8] For the design of our molecular shuttles, we have decided to combine a decyl station with a protonable aromatic subunit (**Figure 1**). Ideally, the pillar[5]arene moiety should form a charge transfer complex with the protonated cationic aromatic moiety, while repulsive interactions should occur in the neutral state. The interaction energy of the pillar[5]arene with the cationic station is expected to be higher than the one between the pillar[5]arene and the decyl station. Therefore, the protonated aromatic station should be preferentially populated. In contrast, in the neutral state, the pillar[5]arene should be preferentially located on the decyl station. For this purpose, we have selected a 1,2,3-triazole unit. Based on preliminary computational studies, this five-membered ring system has an appropriate size to fit within the pillar[5]arene cavity. On the other hand, 1,2,3-triazoles are conveniently prepared by copper-catalyzed alkyne–azide cycloadditions (CuAAC), the so-called click reaction.[9] Concerning the decyl station, the stopper is able to affect its affinity for the pillar[5]arene.[5] For this reason, equivalent systems with different electronic properties have been prepared in order to further evaluate the influence of this structural parameter. Finally, it has been decided to incorporate a tetraethylene glycol spacer between the

N. Becharguia, I. Nierengarten, J.-F. Nierengarten
Laboratoire de Chimie des Matériaux Moléculaires
Ecole Européenne de Chimie, Polymères et Matériaux
Université de Strasbourg et CNRS (UMR 7042, LIMA)
25 rue Becquerel, 67087 Strasbourg, Cedex 2, France
E-mail: iosinska@unistra.fr
nierengarten@unistra.fr

N. Becharguia, R. Abidi
Laboratoire d'Applications de la Chimie aux Ressources et Substances Naturelles et l'Environnement
Faculté des Sciences de Bizerte
Université de Carthage
Zarzouna, Bizerte 7021, Tunisia

A. Sournia-Saquet, B. Delavaux-Nicot
Laboratoire de Chimie de Coordination du CNRS (UPR 8241)
Université de Toulouse (UPS, INPT)
205 Route de Narbonne, 31077 Toulouse, Cedex 4, France
E-mail: beatrice.delavaux@lcc-toulouse.fr

E. Wasielewski
Plateforme RMN Cronenbourg
Université de Strasbourg et CNRS (UMR 7042 LIMA)
Ecole Européenne de Chimie, Polymères et Matériaux
25 rue Becquerel, 67087 Strasbourg, Cedex 2, France

Supporting information for this article is available on the WWW under https://doi.org/10.1002/ceur.202400115

Research Article
doi.org/10.1002/ceur.202400115

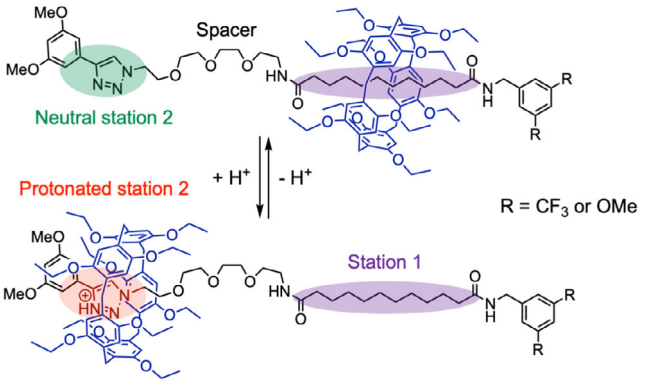

Figure 1. Proposed molecular design for the pillar[5]arene-based molecular shuttles.

two stations. As shown previously, pillar[5]arenes have effectively no particular affinity for oligoethylene glycol stations in organic solvents.[4]

2. Results and Discussion

2.1. Synthesis

The preparation of the pillar[5]arene-containing molecular shuttles is depicted in **Scheme 1**. The synthetic approach to prepare **1a** and **1b** relies on the stopper exchange reaction between readily available rotaxane building blocks bearing an activated pentafluorophenyl ester group[5,10] and an amine reagent equipped with the protonable 1,2,3-triazole subunit. For this purpose, the necessary amine building block **4** was prepared by a CuAAC reaction to generate the 1,2,3-triazole subunit. Treatment of alkyne **2** with azide **3** in the presence of $CuBr.SMe_2$ in CH_2Cl_2 at room temperature afforded the desired amine reagent (**4**) in 85% yield. Subsequent reaction with rotaxanes **5a** and **5b** in tetrahydrofuran (THF) at room temperature gave the targeted molecular shuttles **1a** and **1b** in 93% and 79% yields, respectively. As the stopper exchange reaction occurred through an addition–elimination mechanism, the rotaxane structure is fully preserved during these chemical transformations.[10,11] For comparison purposes, the model compounds depicted in **Figure 2** were also prepared (see Supporting Information).

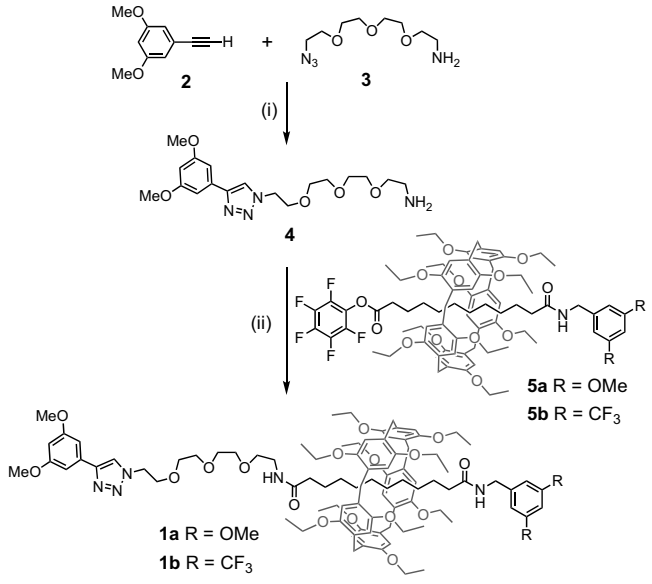

Scheme 1. Preparation of molecular shuttles **1a–b**. *Reagents and conditions*: i) $CuBr.SMe_2$, CH_2Cl_2, and rt (85%). ii) Et_3N, THF, and rt (**1a**, 93%; **1b**, 79%).

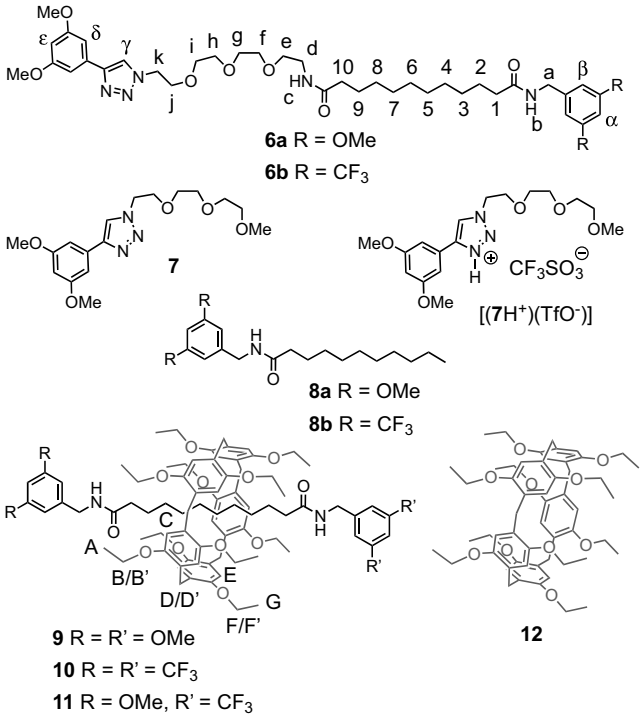

Figure 2. Model compounds and arbitrary numbering used for the attribution of the ^1H NMR spectra.

2.2. Characterization of the New Compounds in the Neutral State

The structure and purity of all the new compounds were confirmed by nuclear magnetic resonance (NMR) spectroscopy, mass spectrometry and elemental analysis. The ^1H NMR spectra of compounds **1a–b** and **6a–b** recorded in CD_2Cl_2 at 298 K are shown in **Figure 3**. When compared to axle **6a–b**, a dramatic shielding of all the signals arising from the decyl chain is observed in the corresponding rotaxanes (**1a–b**) due to the ring current effect of the pillar[5]arene hydroquinone subunits on the axle's CH_2 moieties.

Comparison of **1a** and **1b** reveals significant differences in chemical shifts for the signals of H(1–10). The average position of the macrocyclic component on the decyl chain must be therefore different in **1a** and **1b**. Indeed, the shielding effect is more important for the resonances of H(1–5) in **1b** when compared to **1a**, while an opposite trend is observed for H(6–10). As recently shown for rotaxanes **9–11**, the average position of the electron-rich pillar[5]arene on the decyl station is sensitive to the nature of the

Research Article
doi.org/10.1002/ceur.202400115

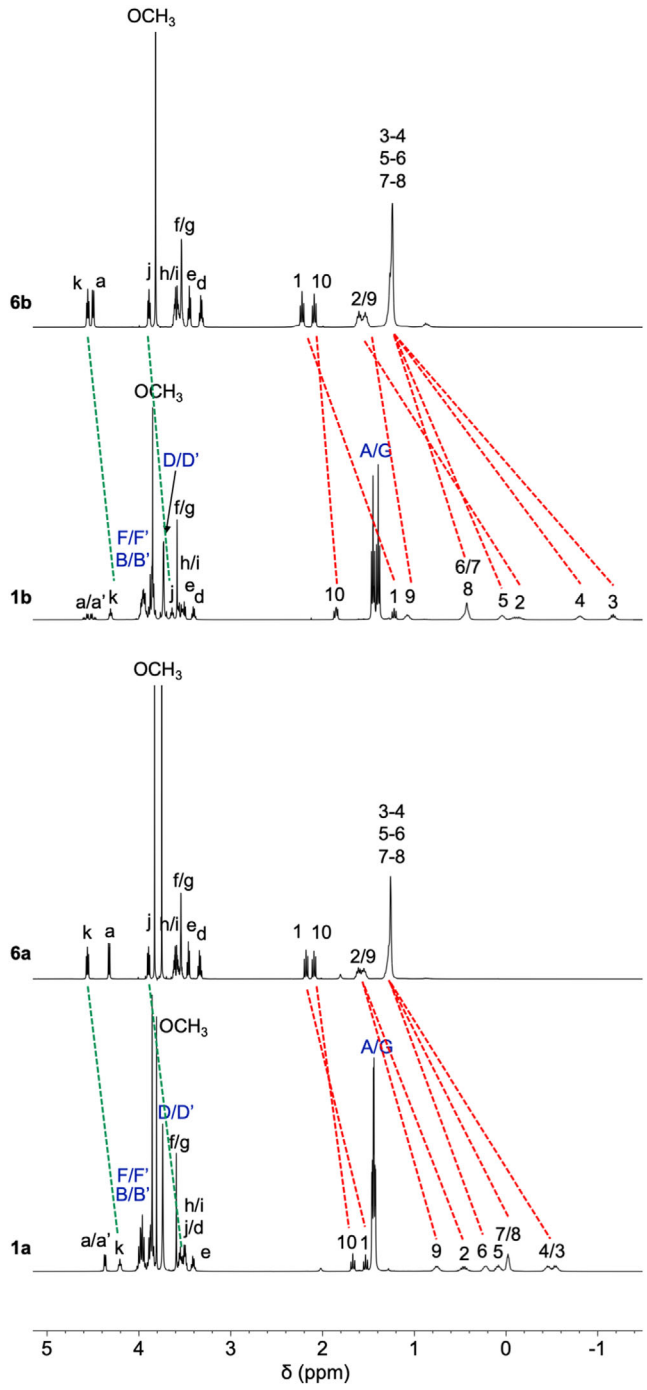

Figure 3. Aliphatic region of the ^{1}H NMR spectra (CD_2Cl_2, 500 MHz) recorded for **1a–b** and **6a–b** at 298 K (for the full spectra, see Figure S1, Supporting Information). For the comparison of the rotaxane with the corresponding axle, changes in chemical shift of the signals arising from the decyl chain station and the triazole station are highlighted in red and green, respectively.

benzylic amide stopper.[5] Weak through-space donor–acceptor interactions between the bis(trifluoromethyl)phenyl moiety and the pillar[5]arene contribute to stabilize conformations in which the macrocycle is close to its electron-deficient stopper in **1b**. In contrast, the attractive interactions are weaker if any in the case of **1a** with an electron-rich terminal stopper. As a result, the position of the macrocycle is distributed more homogeneously over its decyl station in the case of **1a**.

Close inspection of the chemical shifts of some signals arising from protons of the triazole station in **1a–b** and **6a–b** revealed also an upfield shift. Nevertheless, the shielding effect is by far less important than the one observed for the signals of the methylene groups of the decyl station. This observation suggests however that the triazole station is likely partially occupied in **1a–b** under these conditions (CD_2Cl_2, 298 K). This prompted us to record the ^{1}H NMR spectra of **1a–b** at different temperatures. For comparison purposes, the ^{1}H NMR spectra of **6a–b** were also recorded at different temperatures. While no changes of chemical shift could be observed for the signals of axles **6a–b** as a function of the temperature between 298 and 208 K, significant changes were detected for rotaxanes **1a–b** (Figure S1, Supporting Information). For both **1a** and **1b**, the signals arising from the triazole station are downfield shifted by lowering the temperature. At the same time, the signals of the decyl station are upfield shifted. The decyl station is actually more and more populated by decreasing the temperature. Based on the pseudo-coalescence observed for the signals of the OCH_2 substituents of the macrocycle, it was possible to estimate the free energy of activation ($\Delta G^{\ddagger}$) for the dynamic exchange at the coalescence temperature ($T_c = 223$ K). The $\Delta G^{\ddagger}$ values thus obtained for the shuttling of the pillar[5]arene between the decyl and triazole stations were found similar for **1a** and **1b** (46 ± 1 kJ mol^{-1}). By following the chemical shift of the signals observed for the protons of both stations as a function of the temperature, it appears that no changes could be observed for temperatures below T_c (Figure S2, Supporting Information). Therefore, the pillar[5]arene moiety does not exchange its position between the two stations by gliding motions below this temperature. On the other hand, transfer of the chiral information from the macrocycle to the diastereotopic methylene protons H(a/a′) is more and more effective for both **1a** and **1b** when lowering the temperature. This is also in complete agreement with a higher probability of presence of the chiral macrocycle on the decyl station close to H(a/a′) when the temperature is decreased. The chemical shifts of the resonances observed for H(γ) and H(k) are also the same below 223 K for both **1a** and **1b**. The δ values correspond exactly to the one observed for the same protons in the ^{1}H NMR spectra of axles **6a** and **6b** recorded under the same conditions. Obviously, the triazole station is not occupied anymore at temperature below 223 K. The pillar[5]arene is therefore totally located over the decyl station of **1a–b** under these conditions. From an energetic point of view, the difference of energy between the two co-conformers can be estimated higher than 10 kJ mol^{-1} corresponding to a 99.5:0.5 relative population at 223 K based on a Maxwell–Boltzmann analysis. By increasing the temperature, the shielding observed for the resonances of H(γ) and H(k) is less important for **1b** when compared to **1a**, thus indicating a much lower population of co-conformers in which the pillar[5]arene is located over the triazole station in **1b**. This is in perfect agreement with stronger attractive interactions between the pillar[5]arene and the bis(trifluoromethyl)phenyl stopper when compared to the dimethoxyphenyl one.

Research Article
doi.org/10.1002/ceur.202400115

2.3. Binding Studies

To fully understand the behavior of molecular shuttles **1a–b**, the formation of host–guest complexes between pillar[5]arene **12** and appropriate model compounds was also investigated. The association constants (K_A) for the 1:1 complexes were estimated in $CDCl_3$ at 298 K on the basis of the complexation-induced changes in chemical shift by using curve fitting analysis. While no binding could be evidenced under these experimental conditions for model triazole **7**, the formation of inclusion complexes was clearly evidenced for **8a–b** and [(**7**H$^+$)(TfO$^-$)]. The K_A values derived from ^{1}H NMR binding studies together with the corresponding Gibbs free energy of complexation (ΔG^0) values are listed in **Table 1**. As already reported,[5] the nature of the substituents of the terminal benzylic groups of guests **8a** and **8b** have an influence on the K_A values. The formation of the host–guest complex is effectively more favorable for the guest with the electron-deficient bis(trifluoromethyl)benzyl substituent owing to the occurrence of attractive interactions with the electron-rich pillar[5]arene host. As the macrocycle has no affinity for triazole **7**, the preferential position observed for the macrocyclic moiety over the decyl station in **1a–b** is clearly explained. In contrast, the affinity of the model guest for the pillar[5]arene is switched on upon protonation. Based on the relative K_A values obtained for the binding of host **12** with guests [(**7**H$^+$)(TfO$^-$)] and **8a–b**, protonation of molecular shuttles **1a–b** should dramatically influence their conformational equilibria.

2.4. Protonation of the Model Compounds

Before investigating the protonation of **1a–b**, the pK_a(BH$^+$) value of the 1,2,3-triazole station was estimated by following a theoretical method successfully applied to a series of aromatic *N*-heterocyclic compounds (see ESI).[12] The neutral and the protonated forms of 1-methyl-4-(3,5-dimethoxyphenyl)-1,2,3-triazole were calculated at the B3LYP/6-311 + G(2df,2p) level using the conductor-like polarizable model approach[13] with the dielectric constant of water. Calculations were also performed on 1-methyl-4-phenyl-1,2,3-triazole for which a pK_a value is available in the literature (0.05).[14] The 1,2,3-triazole ring contains two basic sp^2-hybridized nitrogen atoms and protonation is more favorable on the more electron-rich N(3) position (Figure S3, Supporting Information). This is fully consistent with experimental and theoretical data reported in the literature for related 1,2,3-triazole derivatives.[14] The basicity of 1-methyl-4-(3,5-dimethoxyphenyl)-1,2,3-triazole and 1-methyl-4-phenyl-1,2,3-triazole was found similar thus showing that the *meta*-substituents of the phenyl group are only playing a minor role (Table S1, Supporting Information). Importantly, the pK_a(BH$^+$) of 1-methyl-4-(3,5-dimethoxyphenyl)-1,2,3-triazole is one to two orders of magnitude higher when compared to pK_a(BH$^+$) values experimentally determined for aliphatic amides in aqueous H_2SO_4.[15] As a result, the first protonation of molecular shuttles **1a–b** and axles **6a–b** containing one triazole moiety and two amide subunits should selectively occur on the triazole station. To fully confirm this selectivity, the protonation of axles **6a–b** and model compound **7** lacking the amide functions was investigated by ^{1}H NMR and ultraviolet-visible (UV–Vis) spectroscopies. Successive addition of trifluoroacetic acid (TFA) to a $CDCl_3$ solutions of **6b** and **7** resulted in similar chemical shift changes for the signals of the 4-(3,5-dimethoxyphenyl)-1,2,3-triazole moiety (Figure S4, Supporting Information). In particular, continuous upfield shifts of the resonance of H(δ) and downfield shifts of the resonances of H(γ) and H(ε) were evidenced in both cases during the titrations. In contrast, the signals of the CH_2 groups neighboring the amide functions of **6b** were only marginally affected by the addition of TFA. All these observations suggest that protonation of **6b** occurs effectively at the triazole N(3) atom as in the case of **7**. Protonation of **7** and **6a–b** was further investigated by UV–Vis spectrophotometric titrations (Figure S5, Supporting Information). As shown in **Figure 4**, the UV–Vis spectra of **7** and **6b** changed substantially upon addition of TFA. A clear isosbestic point is observed at 305 and 301 nm for **7** and **6b**, respectively, thus revealing an equilibrium between two well-defined species in both cases. The similar behavior observed for **7** and **6b** upon addition of TFA further supports the selective protonation of **6b** at the triazole N(3) atom.

Table 1. Association constants (K_A) for the 1:1 complexes obtained from host **12** and guests **8a–b**, **7**, and [(**7**H$^+$)(TfO$^-$)] and the corresponding Gibbs free energy of complexation (ΔG^0).

Guest	8a	8b	7	[(7H$^+$)(TfO$^-$)]
K_A [M^{-1}][a]	2.4(1)[b]	6.6(1)[b]	–[c]	7.2(1)
ΔG^0 [kJ mol^{-1}]	−2.1	−4.6	–	−4.9

[a]Values derived from ^{1}H NMR binding studies performed in $CDCl_3$ at 298 K. [b]From Ref. [5]. [c]No binding under these conditions.

2.5. Protonation of Molecular Shuttles 1a–b

^{1}H NMR titrations of **1a** and **1b** were carried out with TFA in $CDCl_3$ at 298 K (**Figure 5** and Figure S6, Supporting Information). Continuous changes in chemical shifts were evidenced for most of the signals upon the successive additions of TFA. At the same time, a substantial broadening was also observed, in particular for the signals arising from the triazole and the decyl stations. The apparent downfield shift of all the signals of the decyl chain upon protonation of the triazole moiety suggests that the pillar[5]arene moiety has a lower probability of presence over the decyl station upon protonation of **1a–b**. This view is also supported by the evolution of the signal of the benzylic diastereotopic protons during the titration. In the neutral state, a doublet of AB is observed owing to the proximity of the chiral pillar[5]arene subunit. At the end of the titration, the transfer of the chiral information is vanished and a doublet is seen for H(a/a′). Obviously, the probability of presence of the macrocycle near H(a/a′) is significantly reduced upon protonation of the triazole station. All these observations are consistent with a conformational change of **1a–b** upon protonation. Importantly, addition of an excess of triethylamine (Et_3N) at the end of the titration restored the initial state of **1a–b,** thus showing the reversibility of the process (Figure 5).

Research Article
doi.org/10.1002/ceur.202400115

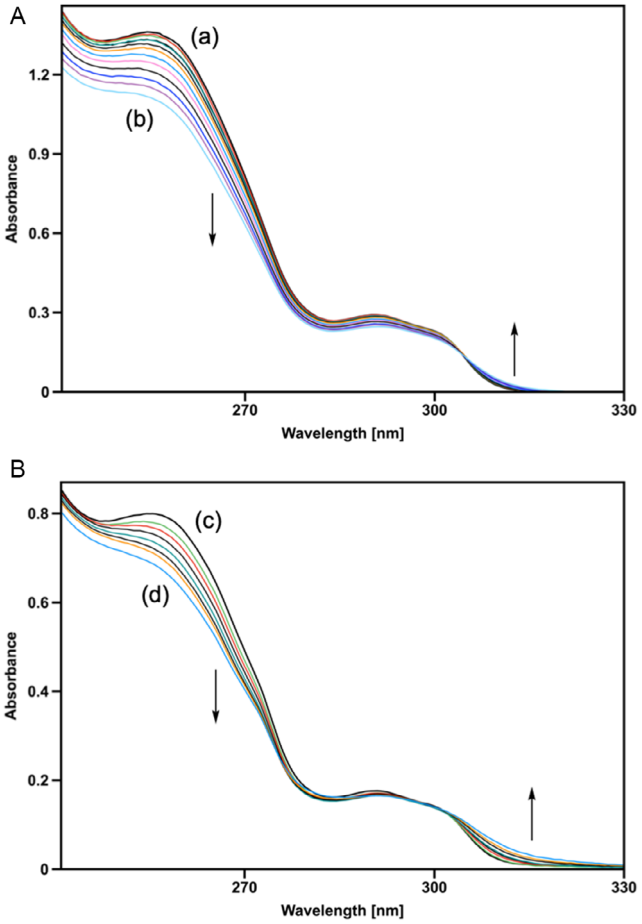

Figure 4. UV–Vis spectrophotometric titrations of A) **7** and B) **6b** with TFA in $CHCl_3$ at 298 K (d = 0.1 cm; a) [**7**] = 5.07×10^{-4} M; b) [TFA]/[**7**] = 65; c) [**6b**] = 6.10×10^{-4} M; and d) [TFA]/[**6b**] = 227).

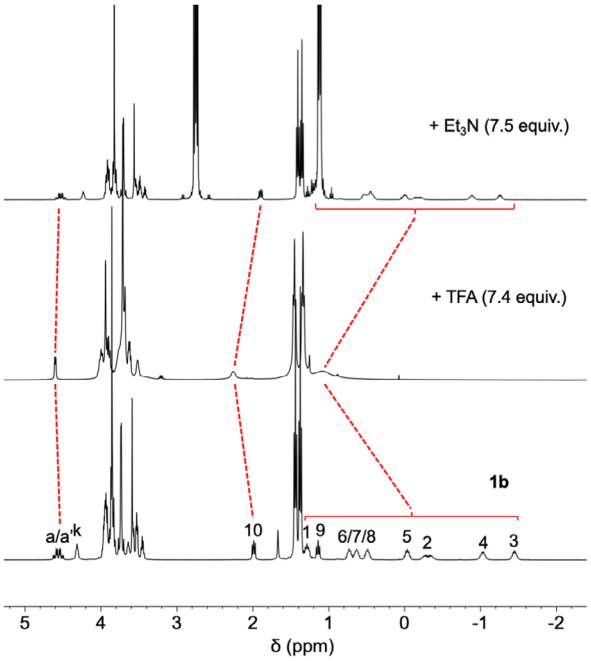

Figure 5. Aliphatic region of the ^{1}H NMR spectra ($CDCl_3$, 400 MHz, 298 K) of **1b**, **1b** after addition of TFA (7.4 equiv.), and neutralization by addition of Et_3N showing the reversibility of the conformational changes (for the full spectra, see Figure S6, Supporting Information).

Owing to the broadening of the signals of **1a–b** during the titrations with TFA, it was difficult to derive clear information about their conformations in the protonated state. This prompted us to prepare the triflate salts of **1a–b** by treatment with a stoichiometric amount of TfOH. For comparison purposes, [(**6a**H$^+$)\(TfO$^-$)] and [(**6b**H$^+$)(TfO$^-$)] were also prepared from **6a** and **6b**, respectively. The use of a strong acid like TfOH allows the total protonation of the triazole station of **1a–b** and **6a–b**. This is essential for a non-ambiguous conformational analysis of [(**1a**H$^+$)(TfO$^-$)] and [(**1b**H$^+$)(TfO$^-$)]. The ^{1}H NMR spectra of [(**1a–b**H$^+$)(TfO$^-$)] and [(**6a–b**H$^+$)(TfO$^-$)] recorded in $CDCl_3$ at 298 K are depicted in Figure S7, Supporting Information. While all the signals of protonated axle [(**6a–b**H$^+$)(TfO$^-$)] are well resolved under these conditions, the spectra recorded for rotaxane (**1a–b**H$^+$)(TfO$^-$) are characterized by the broadening of the signals arising from the CH_2 moieties of the decyl station [H(1–10)]. Similarly, resonances of H(i–k) and H(γ,β,ε) are particularly broad and could not be clearly detected in the ^{1}H NMR spectrum of [(**1a–b**H$^+$)(TfO$^-$)] recorded at room temperature. These observations suggest that the pillar[5]arene is exchanging its position between the decyl and the triazolium stations in [(**1a**H$^+$)(TfO$^-$)] at a rate close to the NMR timescale at 298 K. Clearly, the triazolium station plays a major role in the conformation of protonated molecular shuttles [(**1a**H$^+$)(TfO$^-$)] and [(**1b**H$^+$)(TfO$^-$)].

To fully understand their behavior, variable temperature NMR studies were carried out. A reversible narrowing of most of the broad signals was observed by increasing the temperature, and the ^{1}H NMR spectra of [(**1a**H$^+$)(TfO$^-$)] and [(**1b**H$^+$)(TfO$^-$)] recorded in $C_2D_2Cl_4$ at 373 K are well resolved (Figure S8, Supporting Information). Under these conditions, dynamic gliding motions allowing the macrocycle to shuttle back and forth between the two stations are faster than the NMR timescale. While confirming the dynamic exchange, the ^{1}H NMR spectra recorded at high temperature are not very informative concerning the population of the different possible co-conformers. ^{1}H NMR spectra of [(**1a**H$^+$)(TfO$^-$)] and [(**1b**H$^+$)(TfO$^-$)] were also recorded in CD_2Cl_2 at low temperature. As shown in **Figure 6**, a clear coalescence is observed at 243 K, and the two co-conformers of [(**1a**H$^+$)(TfO$^-$)] are clearly distinguished at lower temperatures. In other words, the dynamic exchange between co-conformers A and B is slower than the NMR timescale under these conditions.

The $\Delta G^{\ddagger}$ value derived from the coalescence of the signals arising from the aromatic protons of the pillar[5]arene moiety is 49 ± 1 kJ mol^{-1}. Based on the integration, the relative proportion of the two co-conformers is 67:33 at 223 K, the major co-conformer being the one in which the triazolium station is occupied (co-conformer B). A Boltzmann population analysis at 223 K revealed a difference of energy of 1.0 kJ mol^{-1} between the two conformations. A similar behavior was also evidenced for [(**1b**H$^+$)(TfO$^-$)] (Figure S9, Supporting Information). However, conformer A is favored in this particular case. At 223 K, a 62:38 ratio was deduced

Research Article
doi.org/10.1002/ceur.202400115

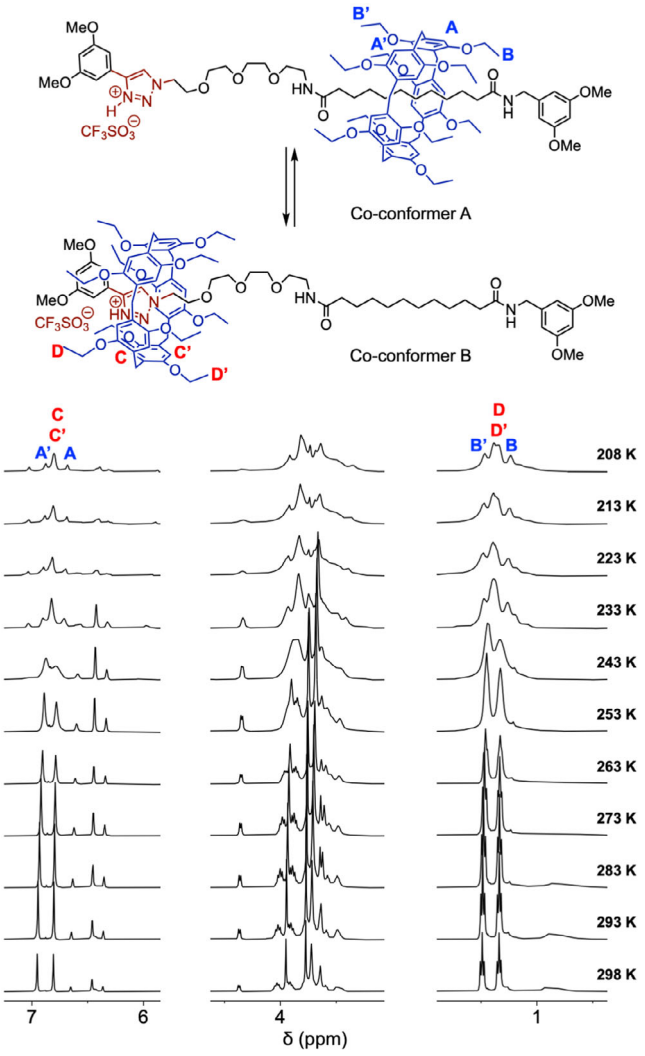

Figure 6. Selected region of the ^{1}H NMR spectra (CD_2Cl_2, 400 MHz, 298 K) of [(**1a**H$^+$)(TfO$^-$)] recorded at different temperatures (for the full spectra, see Figure S9A, Supporting Information).

from the integration corresponding to a difference of energy of 0.9 kJ mol^{-1}. Based on the coalescence of the signals arising from the aromatic protons of the pillar[5]arene moiety, a $\Delta G^{\ddagger}$ value of 50 ± 1 kJ mol^{-1} was obtained for the dynamic exchange between co-conformers A and B. Finally, deprotonation of [(**1a**H$^+$)(TfO$^-$)] and [(**1b**H$^+$)(TfO$^-$)] was investigated by UV–Vis spectrophotometric titrations with Et_3N as a base (Figure S10, Supporting Information). Continuous changes were observed in the UV–Vis spectra upon addition of Et_3N. A clear isosbestic point is also observed, thus revealing an equilibrium between two well-defined species, namely [(**1a–b**H$^+$)(TfO$^-$)] and **1a–b**. The absorption spectrum obtained at the end of the titration is effectively the same as the one recorded for compound **1a–b** in the same solvent.

The conformational equilibria of molecular shuttles **1a–b** in their neutral and protonated state were fully elucidated by variable temperature NMR studies. A summary of all the experimental findings is depicted in **Figure 7**.

In their neutral state, the decyl station of **1a–b** is largely favored over the triazole one. Upon protonation of **1a–b**, the affinity of the resulting triazolium station for the pillar[5]arene is significantly increased. As a result, protonation triggers significant conformational changes. Actually, the pillar[5]arene is exchanging its position between the two available stations at temperatures higher than 243 K, and the relative population of the two possible co-conformers of [**1a–b**H$^+$] is significantly influenced by the *meta*-substituents of the terminal benzylic amide group of the decyl station. This is fully consistent with the influence of the amine stoppers on the K_A values obtained from the binding studies of pillar[5]arene **12** and model compounds **8a–b**. The formation of the inclusion complex is effectively more favorable for guest **8b** with the electron-deficient bis(trifluoromethyl) benzyl substituent. The difference in Gibbs free energy ($\Delta\Delta G^0$) between **8a** and **8b** is 2.5 kJ mol^{-1} under the experimental conditions used for the binding studies ($CDCl_3$, 298 K). This quite small energy difference is however sufficient to significantly influence the Maxwell–Boltzmann distribution of the different possible co-conformers of [**1a–b**H$^+$] and is consistent with a higher population of the decyl station in the case of [**1b**H$^+$] when compared to [**1a**H$^+$]. The effect of such a subtle structural difference could be evidenced because the triazolium station has an affinity similar to that of the different decyl stations. This is fully consistent with the K_A values derived for the binding of pillar[5]arene **12** with model compounds **8a–b** and [(**7**H$^+$)(TfO$^-$)]. Overall, the gliding motions of the pillar[5]arene occur over the full length of its molecular axle in protonated [**1a–b**H$^+$], while such molecular motions are largely limited over the decyl stations in unprotonated **1a–b**. The perfectly reversible protonation/deprotonation of these molecular shuttles allows therefore to control the amplitude of the oscillations of the macrocyclic component along its axle moiety.

2.6. DFT Calculations

In order to fully understand the interactions of the pillar[5]arene moiety with its different stations in **1a–b**, density functional theory (DFT) calculations were carried out with appropriate fragments. Specifically, the structure of the host–guest complexes resulting from the association of pillar[5]arene **12** with octane (**Oct**), 1-methyl-4-(3,5-dimethoxyphenyl)-1,2,3-triazole (**L**), and triazolium (**L**H$^+$) were optimized at the ωB97X-D/6-31G* level (see ESI). The frontier molecular orbitals (FMOs) of **12**, [**12.Oct**], [**12.L**], [**12.L**H$^+$], **Oct**, **L**, and **L**H$^+$ are depicted in **Figure 8**. Comparison of the FMOs of **12** and [**12.Oct**] revealed only a marginal effect of the complexation of **Oct** host by the pillar[5]arene. This is consistent with the absence of strong electronic interactions between **12** and **Oct** in the inclusion complex, and the binding is totally dominated by dispersive interactions. In the case of [**12.L**], the lowest unoccupied molecular orbital (LUMO) of [**12.L**] is distributed over the 3,5-dimethoxyphenyl subunit of **L** and the aromatic subunits of **12**. While the LUMO level centered on **L** is destabilized, the part centered on the pillar[5]arene is stabilized. The highest occupied molecular orbital (HOMO) totally localized on the pillar[5]arene moiety is substantially destabilized ($\Delta E = +0.13$ eV). Overall, these observations revealed rather unfavorable electronic interactions between the host and the guest in

Research Article
doi.org/10.1002/ceur.202400115

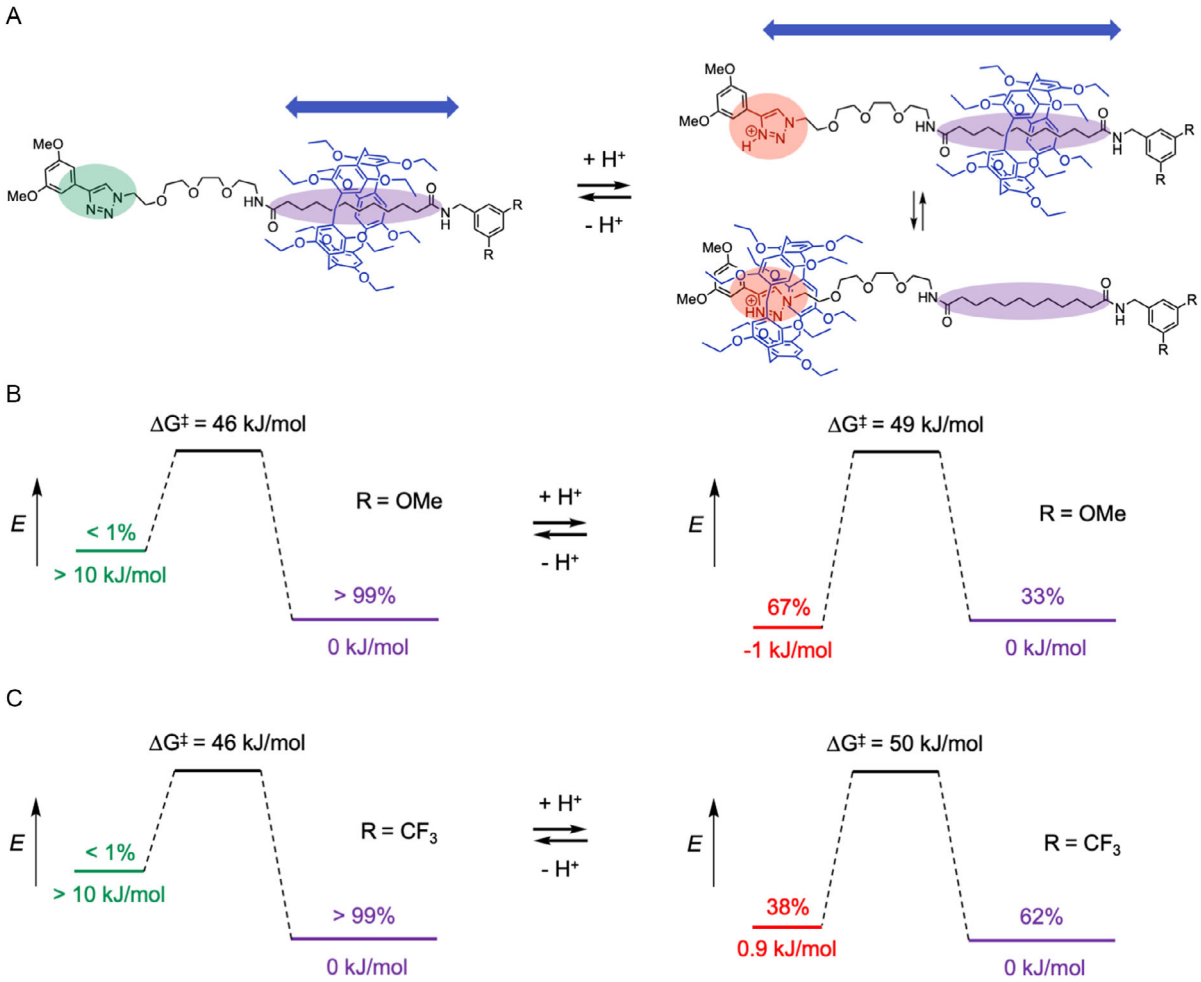

Figure 7. A) As indicated by the blue arrows, gliding motions of the pillar[5]arene moiety occur over the full length of the molecular axle in the protonated state, while such molecular motions are limited over the decyl station in the neutral state. Potential energy diagrams of B) **1a** and C) **1b** in both the neutral and the protonated states deduced from the variable temperature ^{1}H NMR studies; the energy levels and the proportion of the co-conformers are given at 223 K; the free energy of activation ($\Delta G^{\ddagger}$) values for the dynamic exchange are those obtained at the coalescence temperature (223 K in the neutral state and 243 K in the protonated state).

[**12.L**]; therefore, the binding of **L** is mainly governed by dispersive interactions as observed in the case of **Oct**. The situation is totally different for [**12.**LH^+]. In this case, favorable electronic interactions are effectively evidenced by a significative stabilization of the HOMO of **12** ($\Delta E = -0.42$ eV) and a destabilization of the LUMO of LH^+ ($\Delta E = +0.10$ eV) in the host–guest complex. Moreover, with its HOMO fully localized over the pillar[5]arene moiety and its LUMO totally centered on the LH^+ host, [**12.**LH^+] is therefore a charge transfer complex. This was further confirmed by time-dependent DFT (TD-DFT) calculations (see SI and Figure S11, Supporting Information).

The factors controlling the affinity of guest **12** with the different hosts were further analyzed by using the interaction energy decomposition method (Figure S12, Supporting Information).[4] The electronic energy of the host–guest complexes was decomposed into two terms: (i) the distortion energy which corresponds to the energy required for the deformation of the individual components to form the inclusion complex (guest **12** and host **Oct**, **L**, or LH^+) and (ii) the interaction energy which corresponds to the difference between the electronic energies of the two distorted components and the supramolecular complex. The overall energy gain for the formation of the host–guest complex was then evaluated by adding the positive distortion energy to the negative interaction energy. The lowest interaction energy was obtained for inclusion complex [**12.Oct**] in which only van der Waals interactions are possible. For neutral guest **L**, the interaction energy was found 17 kJ mol^{-1} stronger when compared to [**12.Oct**], thus showing more favorable dispersive interactions between the host and the guest in [**12.L**] despite their poor electronic complementarity suggested by the FMOs analysis. However, the overall energy gain is substantially penalized by an important distortion energy (46.4 kJ mol^{-1}). As a result, steric factors explain the more favorable complexation of the octane guest. In the case of molecular shuttles **1a–b**, the preferential location of the pillar[5]arene moiety over the alkyl station results therefore mainly from the limited distortion of the macrocyclic component and electronic factors play only a very minor role. In the case of guest [LH^+], the formation of the host-guest complex with **1** requires also an important distortion of the macrocyclic scaffold. However, the significantly increased interaction energy in [**12.**LH^+] provides

Research Article
doi.org/10.1002/ceur.202400115

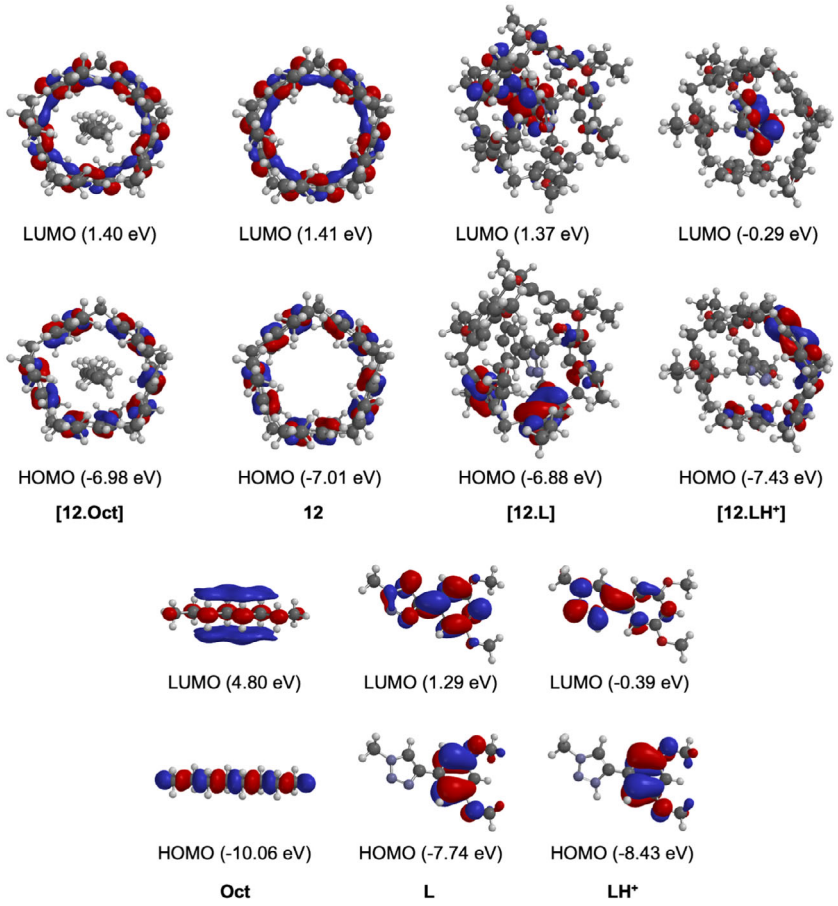

Figure 8. FMOs of octane (**Oct**), 1-methyl-4-(3,5-dimethoxyphenyl)-1,2,3-triazole (**L**), 1-methyl-4-(3,5-dimethoxyphenyl)-1,2,3-triazolium ($\mathbf{LH}^+$), pillar[5]arene **12**, [**12.Oct**], [**12.L**], and [**12.L**H^+] calculated at the ωB97X-D/6-31G* level in THF.

a higher energy gain (-204.6 kJ mol^{-1}). This value certainly overestimates the real energy gain as intimate ion pairs are most likely interacting with the pillar[5]arene guest in nonpolar solvents, thus generating an increased distortion of the guest moiety. On the other hand, basis set superposition error effects are also larger in the case of [**12.L**H^+] when compared to [**12.Oct**] (see SI). Overall, the position of the pillar[5]arene subunit on its axle moiety in **1a–b** and [**1a–b**H^+] results from an interplay between electronic interactions and steric effects. In the neutral state, the conformational preferences are totally dominated by dispersive interactions and steric effects largely prevent occupation of the triazole station in **1a–b**. In contrast, favorable electronic interactions between the protonated triazole moiety and the pillar[5]arene in [**1a–b**H^+] are able to compensate, at least in part, the substantial energy required for the distortion of the macrocyclic scaffold when the triazolium station is populated. As a result, the triazolium station becomes competitive with the decyl station in [**1a–b**H^+].

2.7. Electrochemistry

The electrochemical properties of compounds **1a–b** and [(**1a–b**H^+)(TfO^-)] were determined by cyclic voltammetry (CV) and Osteryoung square wave voltammetry (OSVW).[16] For the sake of comparison, electrochemical measurements were also carried out with model compounds **7**, [(**7**H^+)(TfO^-)], **9**, **10**, **11**, and **12**. All the experiments were performed at room temperature in CH_2Cl_2 solutions containing $n$$Bu_4NBF_4$ (0.10 M) as supporting electrolyte and ferrocene (Fc) as internal reference, with a Pt micro-disk as the working electrode and a saturated calomel electrode (SCE) as a reference. Potential data for all the compounds are collected in **Table 2**. For compounds **9**, **10**, **11**, and **12**, no redox processes could be detected in the cathodic region. In contrast, successive oxidations are observed for all these compounds during the anodic scans (Figure S13, Supporting Information). The two first anodic processes observed in the CV of pillar[5]arene **12** are quasi-reversible and correspond to the stepwise one electron transfer to two of the five hydroquinone subunits of the macrocycle.[17] Additional oxidations are observed by scanning at more positive potentials, these processes are however complex due to adsorption phenomena and the formation of oxidation side products. The electrochemical properties of the corresponding methylated pillar[5]arene derivative have been investigated in details.[18] The third oxidation peak involves three electrons to generate the pentacationic pillar[5]arene, and the fourth peak is a five-electron process related to the oxidation of the pentacation toward quinone products. The electrochemical features of model [2]rotaxanes **9**, **10**, and **11** are characterized by four successive pillar[5]arene-centered oxidations. While the three first

Research Article
doi.org/10.1002/ceur.202400115

Table 2. Electrochemical data of compounds **1a–b**, [(**1a–b**H$^+$)(TfO$^-$)], **7**, [(**7**H$^+$)(TfO$^-$)], **9**, **10**, **11**, and **12** determined by OSWV on a Pt working electrode in CH_2Cl_2 + 0.1 M nBu_4BF_4 at room temperature. Ferrocene is used as internal reference[a),b)].

Compound	E^1_{Red}	E^1_{Ox}	E^2_{Ox}	E^3_{Ox}	E^4_{Ox}	E^5_{Ox}
12[c)]		+1.11[d)]	+1.27[d)]	+1.35	+1.72	
9		+1.09[d)]	+1.28[d)]	+1.48[d)]	+1.63	
10		+1.09[d)]	+1.24[d)]	+1.48	+1.68	
11		+1.07[d)]	+1.25[d)]	+1.46	+1.65	
7		+1.66	+1.91			
[(**7**H$^+$)(TfO$^-$)]	−0.11[e)]	+1.90				
1a		+1.07[d)]	+1.28[d)]	+1.47[d)]	+1.64	
1b		+1.09[d)]	+1.28[d)]	+1.48	+1.68	
[(**1a**H$^+$)(TfO$^-$)]	−0.02[e)]	+1.11	+1.27	+1.47	+1.64	
[(**1b**H$^+$)(TfO$^-$)]	−0.10[e)]	+1.12	+1.25	+1.36	+1.47	+1.68

[a)]OSWVs were obtained using a modulation amplitude of 20 mV, a frequency of 20 Hz, and a step potential of 5 mV. [b)]Potential values in oxidation (E_{Ox}) and reduction (E_{Red}) in Volt versus SCE (Fc^+/Fc is observed at 0.55 ± 0.01 V vs. SCE). [c)]From Ref. [17] [d)]Quasi-reversible processes in CV. [e)]Broad signal.

oxidations correspond to a one-electron transfer, the last oxidation wave involves two electrons. Overall, the five hydroquinone subunits of the pillar[5]arene moiety of the rotaxanes are oxidized in a step-wise manner to generate the corresponding pentacationic species. The redox potentials of the different oxidations of **9**, **10**, and **11** are quite similar, thus showing a limited influence of the amide stopper on the redox properties of the pillar[5]arene moieties. When compared to parent pillar[5]arene **12**, the two first oxidation processes of rotaxanes **9**, **10**, and **11** are only poorly affected by the presence of the alkyl chain within the cavity of the macrocycle. This is fully consistent with the poor influence of the alkyl chain present in the cavity on the FMOs of the pillar[5]arene as evidenced by the DFT calculations. In contrast, the following oxidations suggest a substantial stabilization of the polycationic species in the case of the rotaxanes, and the formation of quinone products seen for **12** is not observed anymore for rotaxanes **9**, **10**, and **11**.

The electrochemical behavior of molecular shuttles **1a–b** is similar to the one observed for model rotaxanes **9**, **10**, and **11** (Figure S14, Supporting Information). Four successive oxidation waves are effectively observed at similar redox potentials. The presence of both the triazole station and the tetraethylene glycol linker has no particular influence on the electrochemical properties of **1a–b**. This suggest that the pillar[5]arene moiety remains located over the decyl station in **1a** and **1b** upon the successive oxidations of the macrocyclic subunit and confirms the stabilization of the polycationic species when an alkyl chain is present in the cavity.

To fully understand the electrochemical properties of protonated molecular shuttles [(**1a–b**H$^+$)(TfO$^-$)], it was important to also investigate the electrochemical properties of model compounds **7** and [(**7**H$^+$)(TfO$^-$)] (Figure S15, Supporting Information). Two oxidation waves are observed at high potential for the neutral compound. Upon protonation of the triazole ring, the system becomes electron-deficient, and a reduction is observed at −0.11 V versus SCE for the triazolium moiety of [(**7**H$^+$)(TfO$^-$)]. On the other hand, only one oxidation wave is evidenced at high potential for [(**7**H$^+$)(TfO$^-$)]. In the cyclic voltammograms recorded for molecular shuttles [(**1a**H$^+$)(TfO$^-$)] and [(**1b**H$^+$)(TfO$^-$)], the diagnostic reduction wave of the triazolium moiety is clearly observed thus confirming the protonation of their *N*-heteroaromatic subunit (Figure S16, Supporting Information).

OSWVs recorded for [(**1a**H$^+$)(TfO$^-$)] and [(**1b**H$^+$)(TfO$^-$)] in the anodic region are shown in **Figure 9**. For comparison purposes, the OSWV of **1a–b** are also represented in Figure 9. Owing to the coexistence of two co-conformers for both [(**1a**H$^+$)(TfO$^-$)] and [(**1b**H$^+$)(TfO$^-$)], their electrochemical behavior is more complicated when compared to **1a** and **1b**. Actually, the first oxidation of the two co-conformers occurs at different potentials. For both protonated molecular shuttles, the first wave (i) is ascribed to the one-electron oxidation of the pillar[5]arene subunit of co-conformer A and the second one (ii) to the simultaneous first pillar[5]arene-centered oxidation of co-conformer B and the oxidation of the pillar[5]arene radical cation of co-conformer A. The two first oxidations are indeed observed at almost the same redox potential for co-conformer A of [(**1a–b**H$^+$)(TfO$^-$)] and the corresponding unprotonated compounds **1a–b**. On the other hand, the first pillar[5]arene-centered oxidation of co-conformer B is shifted to more positive potentials by ≈200 and 160 mV for [(**1a**H$^+$)(TfO$^-$)] and [(**1b**H$^+$)(TfO$^-$)], respectively. This change is fully consistent with the presence of a positively charged triazolium subunit in the cavity of the pillar[5]arene moiety of co-conformer B. It can be noted that similar positive shifts have been already reported for the first oxidation of pillar[5]arene-containing rotaxane in which an imidazolium moiety is located within the cavity of the macrocycle.[19] Upon the first oxidation, the pillar[5]arene radical cation is most likely expelled from the triazolium station due to electrostatic repulsion. In the particular case of [(**1b**H$^+$)(TfO$^-$)], the wave (iii) detected at +1.36 V versus SCE corresponds to the subsequent oxidation of the radical cationic pillar[5]arene. In contrast, no peak separation could be observed in the case of [(**1a**H$^+$)(TfO$^-$)] as the two first oxidations of the pillar[5]arene moiety of co-conformer B occur at very close redox potentials. The triazolium station is totally unoccupied after these oxidations, and the dicationic pillar[5]arene moiety is

Research Article
doi.org/10.1002/ceur.202400115

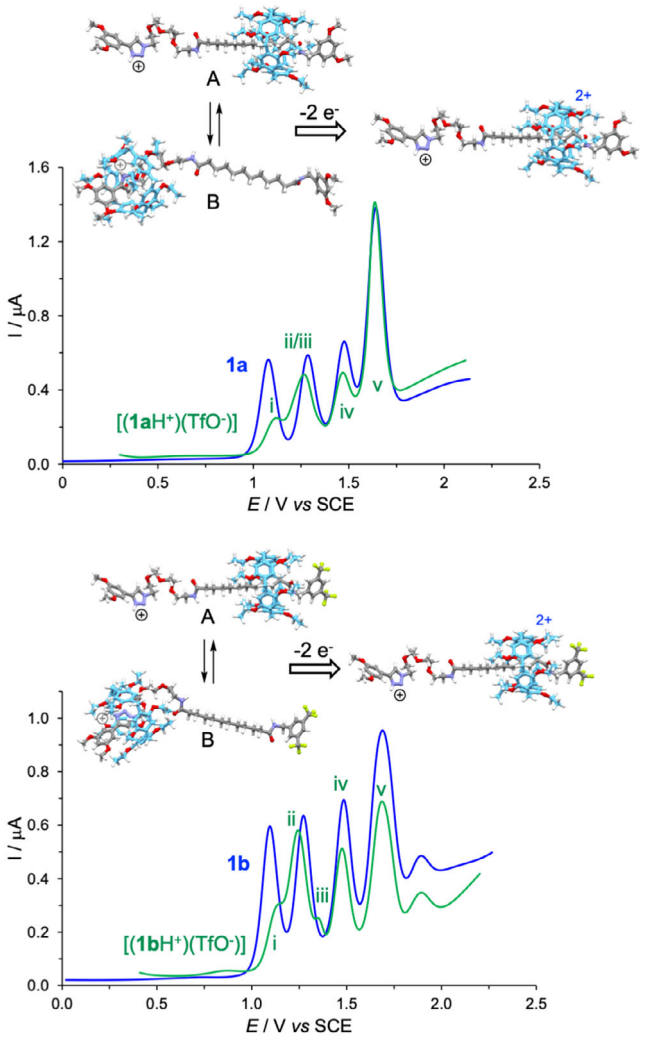

Figure 9. OSWVs (anodic scan; frequency 20 Hz, amplitude 20 mV, step potential 5 mV) of compounds **1a–b** and [(**1a–b**H$^+$)(TfO$^-$)] in CH_2Cl_2 + 0.1 M nBu_4BF_4 at room temperature. Whatever the initial state of [(**1a–b**H$^+$)(TfO$^-$)] (co-conformer A or co-conformer B), only one conformer is present after the two first oxidations as the oxidized macrocycle is expelled from the triazolium station of co-conformer B.

exclusively located on the decyl station whatever the starting conformation (Figure 9). Finally, the two last oxidations (iv and v) are observed at the typical redox potentials of a pillar[5]arene moiety located onto a decyl station. This observation is in full agreement with the proposed conformational reorganization of co-conformer B upon the two first oxidations.

3. Conclusion

New molecular shuttles have been obtained by the functionalization of a rotaxane building block bearing an activated pentafluorophenyl ester stopper with an amine bearing a triazole subunit. Detailed spectroscopic investigations supported by DFT calculations allowed us to fully understand the conformation of these systems. In the neutral state, the pillar[5]arene is almost exclusively located over the decyl station of the rotaxanes. In contrast, upon protonation, the affinity of the triazolium station for the pillar[5]arene is significantly increased. Protonation therefore triggers significant conformational changes. Actually, the pillar[5]arene is exchanging its position between the two available stations and the relative population of the two possible conformers is significantly influenced by the terminal stopper of the decyl station. Overall, the gliding motions of the pillar[5]arene occur over the full length of the molecular axle in the protonated state, while such molecular motions are largely limited over the decyl station in the neutral state. The perfectly reversible protonation/deprotonation of these molecular shuttles allows therefore to control the amplitude of the oscillations of the macrocyclic component along the axle moiety. Moreover, an electrochemical input can also be used to modulate the amplitude of the gliding motions within the protonated rotaxanes. Effectively, upon oxidation, the dicationic pillar[5]arene moiety is only located over the decyl station of the protonated axle.

Supporting Information

The authors have cited additional references within the Supporting Information.[20–24]

Acknowledgements

Financial support from the ANR (projects FastGiant ANR-17-CE07-0012-01 and Pillar ANR-19-CE06-0032), the *Fondation Jean-Marie Lehn*, the LabEx "Chimie des Systèmes Complexes," and the Tunisian Ministry of Higher Education and Scientific Research and Technology is gratefully acknowledged. The authors further thank Dr. J.-M. Strub for the mass spectra and A. Moreau (LCC) for some electrochemical measurements. They also thank Dr. M. Holler for his helpful discussions.

Conflict of Interest

The authors declare no conflict of interest.

Data Availability Statement

The data that support the findings of this study are available in the supplementary material of this article.

Keywords: molecular machines · molecular shuttles · pillar[5]arene · rotaxane · stopper exchange

[1] a) *Molecular Catenanes, Rotaxanes and Knots – A Journey Through the World of Molecular Topology* (Eds: J.-P. Sauvage, C. Dietrich-Buchecker), John Wiley & Sons, Weinheim **1999**; b) C. J. Bruns, J. F. Stoddart, *The Nature of the Mechanical Bond – From Molecules to Machines*, John Wiley & Sons, Hoboken, NJ **2016**.
[2] a) J.-P. Sauvage, *Angew. Chem. Int. Ed.* **2017**, *56*, 11080; b) J. F. Stoddart, *Angew. Chem. Int. Ed.* **2017**, *56*, 11228.
[3] a) V. Balzani, A. Credi, M. Venturi, *Molecular Devices and Machines – A Journey Into the Nano World*, Wiley-VCH, Weinheim **2003**; b) E. R. Kay,

Research Article
doi.org/10.1002/ceur.202400115

D. A. Leigh, *Angew. Chem. Int. Ed.* **2015**, *54*, 10080; c) S. Erbas-Cakmak, D. A. Leigh, C. T. McTernan, A. L. Nussbaumer, *Chem. Rev.* **2015**, *115*, 10081; d) D. A. Leigh, *Angew. Chem. Int. Ed.* **2016**, *55*, 14506; e) S.-J. Rao, Q. Zhang, J. Mei, X.-H. Ye, C. Gao, Q.-C. Wang, D.-H. Qu, H. Tian, *Chem. Sci.* **2017**, *8*, 6777; f) S.-J. Rao, K. Nakazono, X. Liang, K. Nakajima, T. Takata, *Chem. Commun.* **2019**, *55*, 5231; g) Q. Zhang, S.-R. Rao, T. Xie, X. Li, T.-Y. Xu, D.-W. Li, D.-H. Qu, Y.-T. Long, H. Tian, *Chem* **2018**, *4*, 2670; h) S. Corra, M. Curcio, M. Baroncini, S. Silvi, A. Credi, *Adv. Mater.* **2020**, *32*, 1906064; i) M. Boroncini, S. Silvi, A. Credi, *Chem. Rev.* **2020**, *120*, 200; j) C.-S. Kwan, K. C.-F. Leung, *Mater. Chem. Front.* **2020**, *4*, 2825; k) H.-Y. Zhou, Y. Han, C.-F. Chen, *Mater. Chem. Front.* **2020**, *4*, 12.

[4] N. Becharguia, I. Nierengarten, J.-M. Strub, S. Cianférani, M. Rémy, E. Wasielewski, R. Abadi, J.-F. Nierengarten, *Chem. Eur. J.* **2024**, *30*, e202304131.

[5] N. Becharguia, E. Wasielewski, R. Abidi, I. Nierengarten, J.-F. Nierengarten, *Chem. Eur. J.* **2024**, *30*, e202303501.

[6] a) T. Ogoshi, D. Yamafuji, T. Aoki, T.-a. Yamagashi, *Chem. Commun.* **2012**, *48*, 6842; b) S. Dong, J. Yuan, F. Huang, *Chem. Sci.* **2014**, *5*, 247; c) T. Ogoshi, R. Iizuka, D. Kotera, T.-a. Yamagashi, *Org. Lett.* **2015**, *17*, 350; d) P. Langer, L. Yang, C. R. Pfeiffer, W. Lewis, N. L. Champness, *Dalton Trans.* **2019**, *48*, 58; e) T. Ogoshi, D. Kotera, S. Nishida, T. Kakuta, T.-a. Yamagashi, A. M. Brouwer, *Chem. Eur. J.* **2018**, *24*, 6325; f) T. Ogoshi, D. Kotera, S. Fa, S. Nishida, T. Kakuta, T.-a. Yamagishi, A. M. Brouwer, *Chem. Commun.* **2020**, *56*, 10871; g) Y. Wang, Y. Tian, Y.-Z. Chen, L.-Y. Niu, L.-Z. Wu, C.-H. Tung, Q.-Z. Yang, R. Boulatov, *Chem. Commun.* **2018**, *54*, 7991.

[7] K. Kato, S. Fa, S. Ohtani, T. Shi, A. M. Brouwer, T. Ogoshi, *Chem. Soc. Rev.* **2022**, *51*, 3648.

[8] N. Bukhtiiarova, A. Credi, S. Corra, *Chem. Commun.* **2023**, *59*, 13159.

[9] a) V. V. Rostovtsev, L. G. Green, V. V. Fokin, K. B. Sharpless, *Angew. Chem. Int. Ed.* **2002**, *41*, 2596; b) H. C. Kolb, M. G. Finn, K. B. Sharpless, *Angew. Chem. Int. Ed.* **2001**, *40*, 2004.

[10] M. Rémy, I. Nierengarten, B. Park, M. Holler, U. Hahn, J.-F. Nierengarten, *Chem. Eur. J.* **2021**, *27*, 8492.

[11] a) I. Nierengarten, E. Meichsner, M. Holler, P. M. Pieper, R. Deschenaux, B. Delavaux-Nicot, J.-F. Nierengarten, *Chem. Eur. J.* **2018**, *24*, 169; b) I. Nierengarten, J.-F. Nierengarten, *ChemistryOpen* **2020**, *9*, 393.

[12] J.-F. Nierengarten, *J. Porphyrins Phthalocyanines* **2023**, *27*, 1253.

[13] a) T. N. Truong, E. V. Stefanovich, *Chem. Phys. Lett.* **1995**, *240*, 253; b) V. Barone, M. Cossi, *J. Phys. Chem. A* **1998**, *102*, 1995.

[14] a) J. L. M. Abboub, C. Foces-Foces, R. Notorio, R. E. Trifonov, A. P. Volovodenko, V. A. Ostrovskii, I. Alkorta, J. Elguero, *Eur. J. Org. Chem.* **2001**, *2001*, 3013; b) M. Lokov, S. Tshepelevitsh, A. Heering, P. G. Heering, R. Vianello, I. Leito, *Eur. J. Org. Chem.* **2017**, *2017*, 4475.

[15] A. Bagno, G. Lovato, G. Scorrano, *J. Chem. Soc., Perkin Trans.* **1993**, *2*, 1091.

[16] R. G. Compton, C. E. Banks, *Understanding Voltammetry*, Imperial College Press, London **2011**.

[17] a) T. M. N. Trinh, I. Nierengarten, H. Ben Aziza, E. Meichsner, M. Holler, M. Chessé, R. Abidi, C. Bijani, Y. Coppel, E. Maisonhaute, B. Delavaux-Nicot, J.-F. Nierengarten, *Chem. Eur. J.* **2017**, *23*, 11011; b) B. Delavaux-Nicot, H. Ben Aziza, I. Nierengarten, T. M. N. Trinh, E. Meichsner, M. Chessé, M. Holler, P. R. Abidi, E. Maisonhaute, J.-F. Nierengarten, *Chem. Eur. J.* **2018**, *24*, 133; c) M. Steffenhagen, A. Latus, T. M. N. Trinh, I. Nierengarten, I. T. Lucas, S. Joiret, J. Landoulsi, B. Delavaux-Nicot, J.-F. Nierengarten, E. Maisonhaute, *Chem. Eur. J.* **2018**, *24*, 1701; d) G. Boitel-Aullen, L. Fillaud, F. Huet, I. Nierengarten, B. Delavaux-Nicot, J.-F. Nierengarten, E. Maisonhaute, *ChemElectroChem* **2021**, *8*, 3506.

[18] M. Z. Wiloch, E. Kuna, S. Kosiorek, V. Sashuk, M. Jönsson-Niedziolka, *ChemElectroChem* **2021**, *8*, 1507.

[19] N. Pearce, E. S. Davies, N. R. Champness, *Molecules* **2020**, *25*, 1627.

[20] T. M. N. Trinh, I. Nierengarten, M. Holler, J.-L. Gallani, J.-F. Nierengarten, *Chem. Eur. J.* **2015**, *21*, 8019.

[21] T. Ogoshi, K. Kitajima, T. Aoki, S. Fujinami, T.-a. Yamagishi, Y. Nakamoto, *J. Org. Chem.* **2010**, *75*, 3268.

[22] M. D. Tissandier, K. A. Cowen, W. Y. Feng, E. Gundlach, M. H. Cohen, A. D. Earhart, J. V. Coe, T. R. Tutle, *J. Phys. Chem. A* **1998**, *102*, 7787.

[23] a) C. Frassineti, S. Ghelli, P. Gans, A. Sabatini, M. S. Moruzzi, A. Vacca, *Anal. Biochem.* **1995**, *231*, 374; b) C. Frassineti, L. Alderighi, P. Gans, A. Sabatini, A. Vacca, S. Ghelli, *Anal. Bioanal. Chem.* **2003**, *376*, 1041.

[24] Y. Shao, L. F. Molnar, Y. Jung, J. Kussmann, C. Ochsenfeld, S. T. Brown, A. T. B. Gilbert, L. V. Slipchenko, S. V. Levchenko, D. P. O'Neill, R. A. DiStasio, R. C. Lochan, T. Wang, G. J. O. Beran, N. A. Besley, J. M. Herbert, C. Y. Lin, T. V. Voorhis, S. H. Chien, A. Sodt, R. P. Steele, V. A. Rassolov, P. E. Maslen, P. P. Korambath, R. D. Adamson, B. Austin, J. Baker, E. F. C. Byrd, H. Dachsel, R. J. Doerksen, A. Dreuw, B. D. Dunietz, A. D. Dutoi, T. R. Furlani, S. R. Gwaltney, A. Heyden, S. Hirata, C.-P. Hsu, G. Kedziora, R. Z. Khalliulin, P. Klunzinger, A. M. Lee, M. S. Lee, W. Liang, I. Lotan, N. Nair, B. Peters, E. I. Proynov, P. A. Pieniazek, Y. M. Rhee, J. Ritchie, E. Rosta, C. D. Sherrill, A. C. Simmonett, J. E. Subotnik, H. Lee Woodcook, W. Zhang, A. T. Bell, A. K. Chakraborty, D. M. Chipman, F. J. Keil, A. Warshel, W. J. Hehre, H. F. Schaefer, J. Kong, A. I. Krylov, P. M. W. Gill, M. Head-Gordon, *Phys. Chem. Chem. Phys.* **2006**, *8*, 3172.

Manuscript received: December 19, 2024
Revised manuscript received: March 19, 2025
Version of record online: